Journal of Photochemistry and Photobiology A: Chemistry 200 (2008) 364–370

Contents lists available at ScienceDirect

Journal of Photochemistry and Photobiology A: Chemistry

journal homepage: www.elsevier.com/locate/jphotochem

Photovoltaic performance of nanostructured zinc oxide sensitised with xanthene dyes

E. Guillén[a], F. Casanueva[a], J.A. Anta[a,*], A. Vega-Poot[b], G. Oskam[b], R. Alcántara[c], C. Fernández-Lorenzo[c], J. Martín-Calleja[c]

[a] Area de Química Física, Departamento de Sistemas Físicos, Químicos y Naturales, Universidad Pablo de Olavide, 41013 Sevilla, Spain
[b] Departamento de Física Aplicada, CINVESTAV-IPN, Mérida, Yucatán, Mexico
[c] Departamento de Química Física, Universidad de Cádiz, Cádiz, Spain

ARTICLE INFO

Article history:
Received 9 April 2008
Received in revised form 9 July 2008
Accepted 23 August 2008
Available online 3 September 2008

Keywords:
Dye-sensitised solar cells
ZnO nanoparticles
Organic dyes
Xanthene

ABSTRACT

The photovoltaic properties of nanostructured ZnO electrodes prepared from commercially available ZnO nanoparticles (Degussa) and sensitised with xanthene dyes are explored. We have used Eosin Y, Eosin B and Mercurochrome and compared their performance to that of the more common N719 dye. We observe that these dyes efficiently sensitise commercial ZnO nanopowder and yield efficiencies that are very competitive with respect to those provided by N719. Local photocurrent and transmittance measurements as a function of the wavelength confirm the good performance of the xanthene dyes in the absorption maxima. We have prepared polymer-sealed cells and measured the short-circuit current of the devices under continuous illumination at 200 mW/cm^2 corresponding to twice the standard solar light intensity. The organic dyes show very good stability properties under these conditions. The combination of a versatile metal oxide such as ZnO and inexpensive organic dyes should be considered as a promising alternative in the field of dye-sensitised solar cells.

1. Introduction

Dye-sensitised solar cells (DSSCs) based on nanostructured high-bandgap semiconductors have received considerable attention since the seminal work of O'Regan and Grätzel in 1991 [1]. DSSC devices exhibit very attractive features for the photovoltaic industry due to the low cost of the materials and the relative simplicity of their manufacture procedure [2]. The efficient functioning of DSSCs is based on the combination of a mesoporous metal oxide derivatized with an appropriate sensitiser that acts as a light harvester (commonly a ruthenium complex) and an appropriate redox couple (typically I_3^-/I^-). The current efficiency record is 11.1% [3] and large-scale (pilot plant) fabrication of DSSC modules with 6–7% efficiency has been demonstrated [4].

A DSSC consists of a photoanode, an electrolyte solution, and a counter electrode in a sandwich configuration using a polymer separator and sealant. The photoanode is prepared by adsorbing the dye onto a nanostructured, mesoporous metal oxide substrate on a transparent conducting oxide (TCO) electrode. The counter electrode consists of a platinised TCO electrode that is placed on top of the working electrode, separated by a polymer sealant. The device is then filled with a suitable liquid or semi-liquid electrolyte in which the redox couple has been dissolved. Although TiO_2 (anatase) is by far the most utilized semiconductor in DSSCs, ZnO has been also investigated [5]. ZnO exhibits very similar photoelectrochemical and transport properties as TiO_2 and has the additional advantage that it is suitable for the easy fabrication of nanostructures such as nanorods and nanotubes that might improve performance. Nevertheless, the efficiency of ZnO-based solar cells remains far from their TiO_2 counterparts. To our knowledge, the best efficiency for ZnO-based solar cells at 1 sun illumination is 3.4% when an electrohydrodynamic method is utilized [6], and 4.1% when the ZnO film is deposited via a pyrolysis procedure [7]. The low performance of ZnO cells has been ascribed to poor sensitisation with the most common ruthenium-based dyes [5,8–10], which has been attributed to partial dissolution of the ZnO and formation of aggregates with the dye.

On the other hand, it has been reported that ZnO performs particularly well when sensitised with organic dyes such as Eosin Y [11–14], Mercurochrome [15,16] or Rose Bengal [17]. Organic dyes such as these are inexpensive and do not rely on the availability of precious metals such as ruthenium. They also have high extinction coefficients and their molecular structures contain adequate anchoring groups to be adsorbed onto the oxide surface. Moreover,

* Corresponding author.
E-mail address: anta@upo.es (J.A. Anta).

1010-6030/$ – see front matter © 2008 Elsevier B.V. All rights reserved.
doi:10.1016/j.jphotochem.2008.08.015

they are especially interesting when used in combination with ZnO due to the disadvantages of using Ru-based dyes with this oxide [18].

In this paper we present a comparative study of the photovoltaic performance of ZnO nanostructured electrodes sensitised with xanthene dyes and the more common N719 dye. We use nanoparticle suspensions prepared from commercial ZnO powder to fabricate DSSC devices, and their photovoltaic characteristics are measured under simulated sunlight. Special attention is paid to the sensitisation behaviour and the stability of the devices. In addition, in order to ascertain the benefits of the xanthene dyes as suitable candidates to replace Ru-based dyes in ZnO-based cells, we used high light intensity and cells of 1 cm^2 for prolonged testing.

2. Materials and methods

Photoelectrochemical experiments were carried out using dye-sensitised ZnO mesoporous films in a thin layer solar cell. The ZnO films were prepared from commercial colloidal ZnO powder (Degussa VP AdNano®ZnO20) with an approximate nanoparticle size of 20 nm (see Fig. 1.) The powder was mixed with water and ethanol (30:70) and stirred overnight to obtain a colloidal suspension of 30 wt.% ZnO.

The solar cell devices were prepared using the following procedure. The suspension was spread onto a F-doped SnO_2 transparent electrode (TCO15, Hartford Glass Company) with a glass rod and then dried in air. Scotch tape (~50 μm) was used for controlling deposition. The film was then heated to 420 °C for 30 min. The film thickness ranged between 10 and 15 μm after sintering. Sensitisation was performed by immersing the electrodes in ethanolic solutions of the different dyes employed. A concentration of 0.5 mM was used for the Ru-based dye known as N719 (solaronix) and Mercurochrome (Sigma). A concentration of 32 mM was used for Eosin Y and Eosin B (Panreac). Eosin Y was studied both in salt ($C_{20}H_6O_5Br_4Na_2$) and acid form ($C_{20}H_8O_5Br_4$) (Fig. 2). The electrodes were immersed in the sensitising solutions for times ranging from 5 to 270 min.

The counter electrode was prepared by spreading a drop of hexachloroplatinic acid (0.01 M in isopropanol) on the conductive side of another transparent electrode and then annealing at 380 °C for 10 min. The electrolyte solution was prepared by dissolving *tert*-butyl ammonium iodide (TBAI), I_2 and *tert*-butylpyridine (TBP) in propylene carbonate (HPLC grade) with concentrations of 0.5, 0.05 and 0.5 M, respectively. Similar as observed for TiO_2 cells [19], it was found that TBAI lowers the recombination rate and produces larger photovoltages [20]. This is especially important for eosin cells, since in this case TBP was found to remove the dye from the oxide surface.

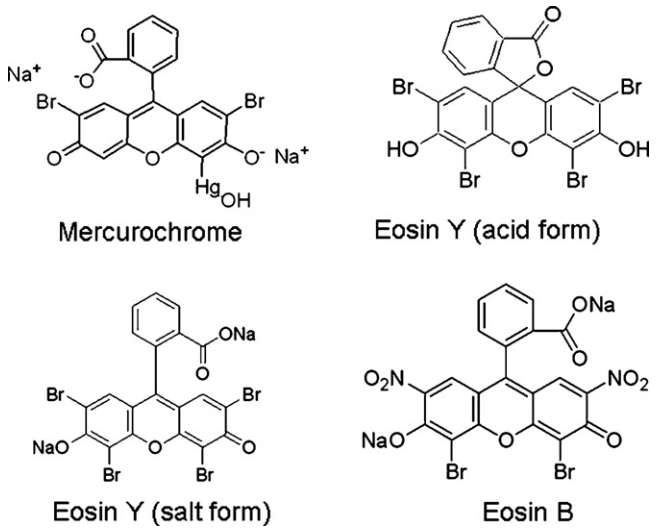

Fig. 2. Molecular structure of the xanthene dyes studied in this work.

The ZnO films were deposited in a rectangular arrangement in order to minimise resistance losses due to the conducting glass. In order to determine the benefits of using new dyes in large-scale applications we performed the study on cells with an active area of 1 cm^2. Permanent cells were fabricated by sealing with Surlyn film (60 μm) heated to 180 °C after sensitisation. Two small holes (1 mm), previously perforated in the counter electrode, were then used to introduce the electrolyte solution. The holes were sealed with Surlyn and a thin glass slide pressed under heat.

UV/vis absorbance spectra were recorded on an Ocean Optics high-resolution spectrophotometer. Short-circuit currents, open-circuit voltages and current–voltage curves were obtained by applying an input voltage to the cell from zero to open-circuit voltage through a Direct Current Accuracy Operational Amplifier. The illumination source was a Thermo Oriel Xenon 450 W arc lamp

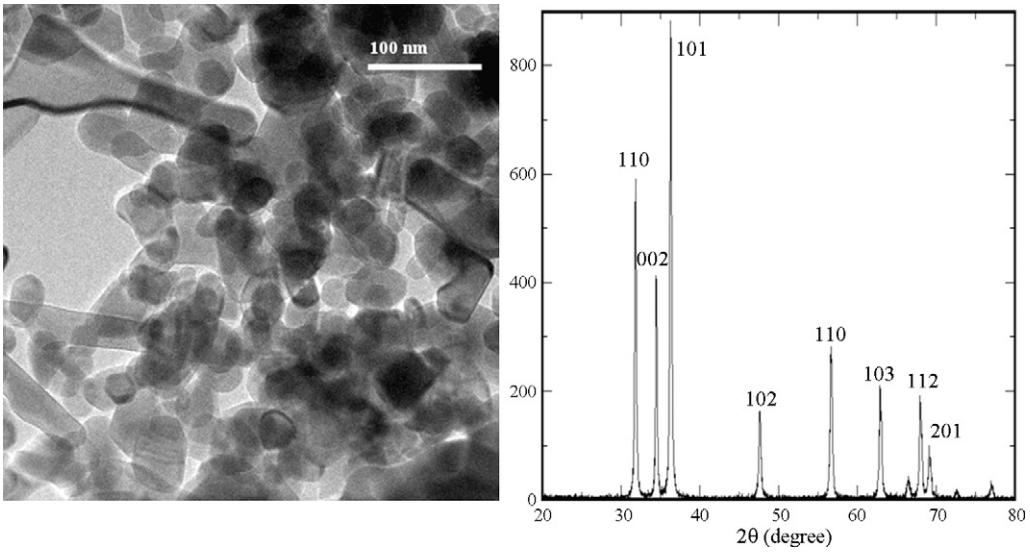

Fig. 1. TEM micrograph and XRD pattern of the Degussa ZnO nanopowder.

coupled to a water filter to remove IR radiation and a 325 nm UV blocking filter. The white light illumination intensity was calibrated to 100 and 200 mW/cm^2 at room temperature using a reference solar cell with temperature output (Oriel, 91150). Incident photon-to-electron conversion efficiencies (IPCE) were measured by means of a 1/8 m monochromator (Oriel). The light intensity was determined as a function of wavelength using a calibrated silicon photodiode (Thorlabs).

The sensitisation efficacy and local photoconversion properties were analyzed by means of the laser beam induced current (LBIC) technique [21–27]. In previous work, a new design for a high-resolution LBIC system was presented, which is based on the application of an optomechanical device to obtain a very small laser spot and minimal geometric distortions in conjunction with a set of mathematical algorithms based on [21,28] internal properties of the samples to perform automatic focalization. In this work, measurements with micrometric resolution were carried out using this versatile computer controlled high-resolution LBIC system [29]. Two different wavelengths were studied: 532 and 632.8 nm. The intensity of the first was fixed at 4.15 μW whereas the 632.8 nm laser was set to 5.10 μW for N719 cells and 515.0 μW for Mercurochrome and eosin cells, where the higher light intensity was needed to obtain similar currents due to the lower absorption of these dyes in the red compared to that of N719. The LBIC experiments were performed on sealed cells and the scanned area was 300 μm × 300 μm. The laser was focused on a surface of 2×10^{-12} m^2.

3. Results and discussion

3.1. Tinction procedure

In the case of ZnO, it has been observed that the time of immersion in the solution of the sensitising dyes is a key factor in the functioning of DSSCs. We have analysed the effect of immersion time for N719 and the xanthene dyes, and the results are presented in Fig. 3. For the N719 dye, there is a critical time of immersion beyond which the cells yield a lower photocurrent, as was previously reported in Ref. [10]. On the contrary, eosin produces currents that do not depend much on the immersion time. Mercurochrome exhibits a similar behaviour to that of N719, at least within the time window studied. The dye is adsorbed rapidly, and upon longer immersion times a systematic decay of the current is observed. Based on these results, the immersion time was set to 1 h for the ruthenium dye, 80 min for the eosin dyes and 40 min for Mercurochrome.

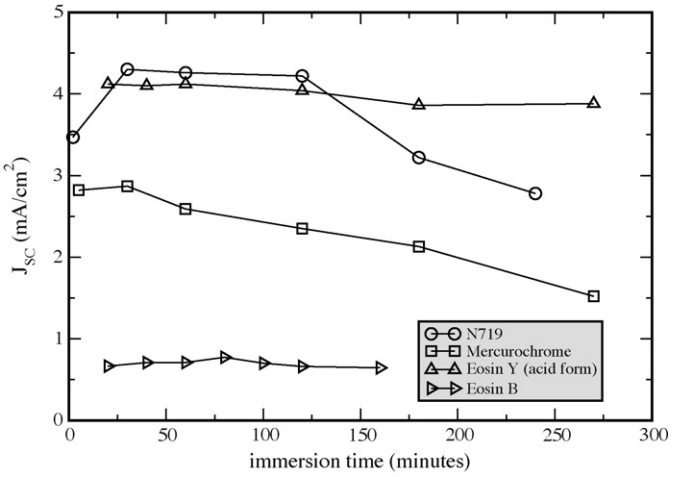

Fig. 3. Short-circuit photocurrent as a function of sensitisation time for the dyes studied in this work under 100 mW/cm^2 illumination.

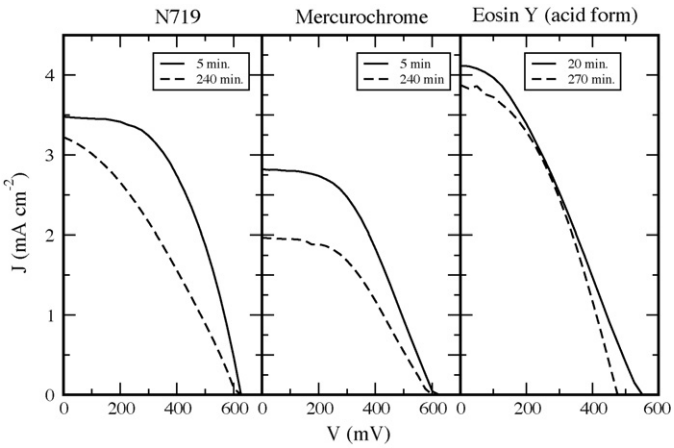

Fig. 4. Current–voltage characteristics of ZnO DSSCs prepared with different dyes for various immersion times in the dye solution.

The immersion time also affects the shape of the current–voltage curve (see Fig. 4). It is observed that the fill factor in the N719 cells decreases with sensitisation time whereas it remains unaffected when the organic dyes are used. In the case of Mercurochrome cells, longer inmersion times reduce only the short-circuit current but the fill factor and open-circuit voltage are not altered. When using eosin the current–voltage curve is virtually independent of the immersion time used to prepare the cells. Although not shown, this feature was observed with all the forms of eosin.

The deterioration of the photocurrent with increasing immersion time has been attributed to partial dissolution of the oxide in the presence of the Ru dye and to the formation of a complex with the Zn^{2+} cations [18,30]. This would explain the reduction of the photocurrent, due to lowering of the effective adsorbed sensitizer concentration, and the fill factor, as a consequence of the increase of the internal resistance upon deterioration of the semiconducting film and the presence of aggregates in the pores. In this work we observe a similar but weaker effect with Mercurochrome although, in this case, the photocurrent reduction is not accompanied by a reduction of the fill factor. This result suggests that ZnO reacts with Mercurochrome. The formation of aggregates of ZnO and Mercurochrome has been mentioned by Hara et al. [16].

3.2. IPCE spectra

Fig. 5 shows the incident photon-to-electron conversion efficiency (IPCE curves) as function of wavelength for the three dyes. The IPCEs were convoluted with the AM1.5 standard photon flux normalized to 100 mW/cm^2 and then integrated between 450 and 700 nm to test the accuracy of the illumination set-up. The result for the photocurrent is then compared with the value obtained under white light illumination with a 400 nm blocking filter. In general, the calculated value is higher than observed experimentally, although the results are within the statistical uncertainty found in the fabrication of the cells (see below). Note also that the photoconversion in the interval 400–450 nm is not considered and this introduces some error that can be important for N719. These results are in agreement with the observation that the cells perform better under real solar illumination, resulting in short-circuit current densities around 10–25% higher than obtained with the lamp.

Mercurochrome and eosins absorb mainly in the 500–550 nm range. When adsorbed on ZnO nanopowder, their action spectra get

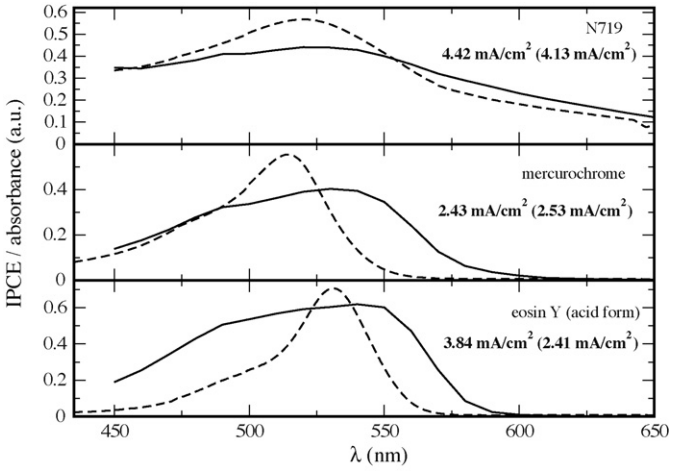

Fig. 5. IPCE (solid lines) and absorbance spectra in ethanolic solution (dashed lines) for the organic dyes considered in this work and N719. The values of the photocurrent shown correspond to the integration between 450 and 700 nm of the IPCE data convoluted with the AM1.5 photon flux at 100 mW/cm^2. In parenthesis, the result of illuminating the cell under white light with a 400 nm blocking filter is indicated.

broader with respect to the absorption curve, so that most of the visible range is covered. A similar behaviour has been reported in Ref. [16], where the broadening of the action spectrum was attributed to the interaction of the ZnO with the dye so that extra energy levels appear in the electronic spectrum of the dye. This "doubling" of the original HOMO and LUMO levels allows for a broadening of the optical absorption spectrum and charge injection, as compared to the absorption spectrum of the isolated dye. A similar effect could be expected for the eosin molecules. Note that the shape of the absorbance and action spectra for N719 are essentially identical, which indicates that the transition energy for electron transfer from the Ru-center to the bpy-ligands is relatively insensitive to the presence of linkage between the carboxyl group and the ZnO surface.

3.3. Current–voltage characteristics

A summary of results for photocurrent and photovoltage results can be found in Fig. 6 and Table 1. Fig. 6 shows average results for

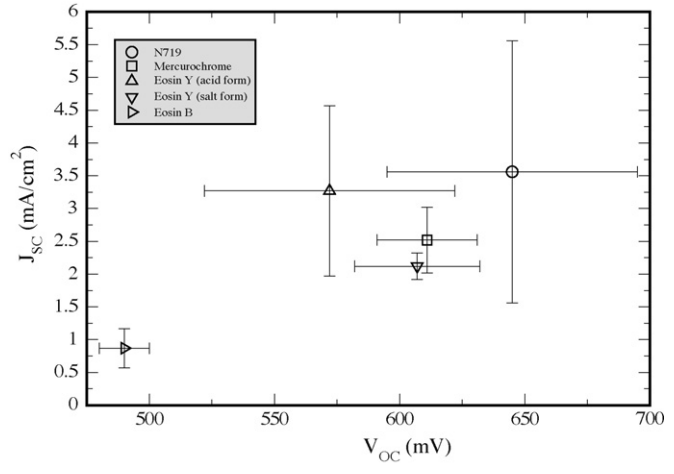

Fig. 6. Summary of photovoltaic characteristics under white light illumination (100 mW/cm^2) for 1 cm^2 ZnO-based DSSCs (J_{sc}: short-circuit current, V_{oc}: open-circuit photovoltage). Error bars result from independent measurements from 5 to 10 cells per dye.

Table 1
Best results for overall efficiencies of 1 cm^2 ZnO-based DSSCs under white light illumination at 100 mW/cm^2 (J_{sc}: short-circuit current, V_{oc}: open-circuit photovoltage, FF: fill factor, η: electric power conversion efficiency)

Dye	J_{sc} (mA/cm^2)	V_{oc} (mV)	FF	η (%)
N719	6.0	701	0.42	1.8
Mercurochrome	3.1	626	0.56	1.1
Eosin Y (acid form)	4.5	551	0.47	1.2
Eosin Y (salt form)	2.7	641	0.60	1.0
Eosin B	1.0	507	0.43	0.15

a series of 5–10 cells per dye, with the respective standard deviation shown as error bars. Reproducibility is not optimal, both in photocurrent and photovoltages. However, it must be noted that we worked with 1 cm^2 cells, which makes achieving good reproducibility more cumbersome. As shown below in the LBIC experiments, there is at least 10–15% variability in the local photocurrent at different points of the film. This variability becomes important when working with large cells.

It is generally observed that the N719 dye produces the best-performing cells, both in current and voltage. However, Mercurochrome cells give values very close to those of the Ru-based dye. Cells prepared with Eosin Y in acid form also provide competitive currents although photovoltages are generally lower. This is most probably due to the absence of TBP in the electrolyte in these cells, as it was found that the presence of TBP results in the removal of eosin from ZnO surface. The eosin in salt form does improve on the photovoltage part, but at the cost of lowering the photocurrent. Eosin B, in contrast, performs rather poorly in comparison with the rest of the dyes. Fill factors are in the range 0.4–0.6 for most cells and the efficiencies ranged between 0.4 and 1.2% for the organic dyes and 1.0–1.8% for N719 cells.

In Fig. 7 the short-circuit current and the open-circuit voltage are shown versus the light intensity for sealed cells with the N-719, Eosin Y (acid), and Mercurochrome dyes. The short-circuit photocurrent is linearly proportional with light intensity up to 200 mW/cm^2 for the three dyes. On the other hand, the open-circuit photovoltage is linear with the logarithm of the light intensity with a slope of ~26 mV, exhibiting ideal diode behaviour for the three dyes studied. These results show that no substantial change is induced in the underlying mechanisms of transport, injection and

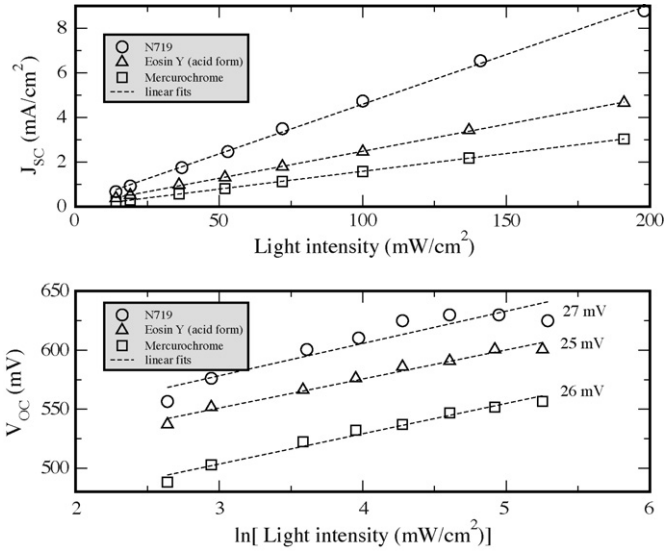

Fig. 7. Light intensity dependence of the short-circuit photocurrent and open-circuit photovoltage for N719, Mercurochrome and Eosin Y (acid form).

Table 2
Photoconversion data as extracted from LBIC experiments

Wavelength (nm)	Dye	Max IPCE (%)	Min IPCE (%)	Mean IPCE (%)	S.D.
532.0	N719	24.4	13.1	19.2	1.2
	Mercurochrome	19.7	9.8	15.1	0.9
	Eosin Y (acid form)	29.1	15.5	20.3	1.2
632.8	N719	4.30	2.87	3.30	0.11
	Mercurochrome	0.159	0.067	0.102	0.014
	Eosin Y (acid form)	0.033	0.024	0.027	0.001

recombination when the illumination intensity is increased up to 200 mW/cm^2.

Permanent cells with increased long-term stability can be prepared by sealing with polymer as explained above. At this point no apparent degradation of the organic dyes is observed as a result of the thermal treatment necessary to prepare the sealed cells (180 °C). In general the sealed cells prepared with Mercurochrome exhibit the best fill-factors, whereas N719 cells tend to deteriorate when the cells are sealed (not shown).

3.4. Local energy conversion performance

The spatial dependence of the efficiency of the cells was evaluated by means of the LBIC technique [21] in combination with transmittance measurements. Results are presented in Tables 2 and 3 and Figs. 8 and 9.

The LBIC mapping technique permits to study simultaneously the local performance of the cells, dye degradation, and the efficacy of the oxide sensitisation. The overall results confirm the good

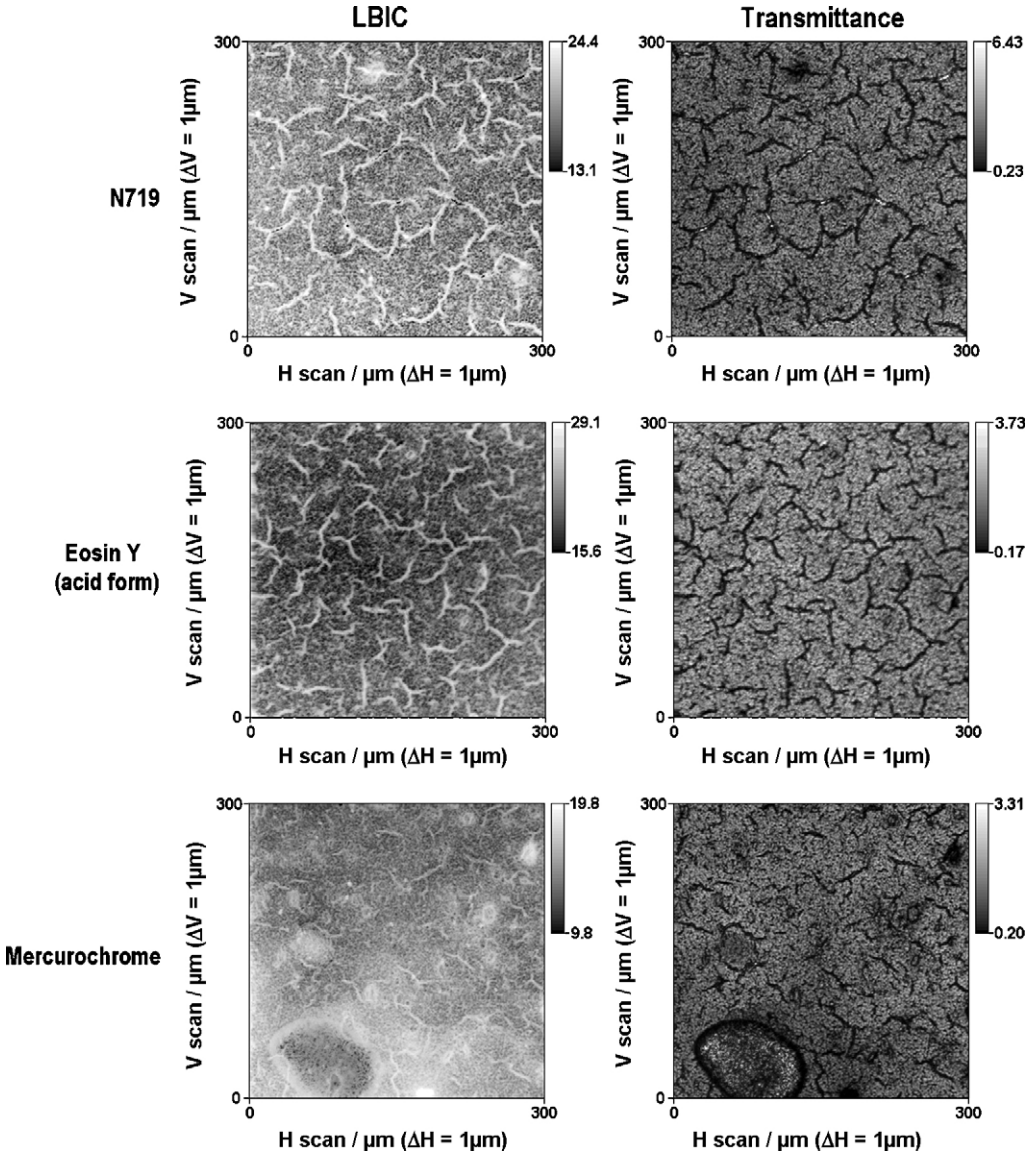

Fig. 8. LBIC and transmittance maps for sealed cells, using the 532 nm laser line. Photoconversion efficiencies (%) and transmittance data (%) are coded using a grey scale, the white being the maximum value in the selected interval.

Table 3
Transmittance data corresponding to the LBIC scans in Table 2

Wavelength (nm)	Dye	Max T (%)	Min T (%)	Mean T (%)	S.D.
532.0	N719	6.4	0.2	1.9	0.8
	Mercurochrome	3.3	0.2	0.9	0.4
	Eosin Y (acid form)	3.7	0.2	1.5	0.5
	No dye	22.9	1.4	7.9	3.1
632.8	N719	47.4	1.7	16.6	7.2
	Mercurochrome	56.2	3.4	16.5	7.4
	Eosin Y (acid form)	59.3	2.5	17.3	6.9
	No dye	50.2	2.6	20.8	7.8

performance of the organic dyes with respect to the Ru-based dyes. The quantum efficiency of the organic dyes is especially impressive at 532 nm, however, the efficiency decreases dramatically when the test is performed at 632.8 nm. These results clearly show that the main reason for the decrease of overall efficiency for DSSCs with the organic dyes when compared to the standard N719, is the poor absorption at wavelengths beyond 600 nm. This conclusion is confirmed by the high value of the transmittance for cells with the organic dyes at 633.8 nm.

For the surface distribution of the local photoconversion performance similar results are observed for the three dyes. The regions of larger photoconversion efficiency are found to correlate well with regions where a stronger light harvesting is detected. To evaluate this effect, transmittance measurements were performed simultaneously with the LBIC measurements (results in Table 3 and Fig. 8). Cross-correlation between both sets of data is presented in Fig. 9.

As can be seen in Fig. 8, the regions of higher conversion efficiency correspond to regions where the transmittance value is lower, and *vice versa*. This indicates that the light harvesting efficiency is the main factor that controls the performance of the cells. This result is further confirmed by Fig. 9, where the quantum efficiency values are plotted versus the transmittance along a straight line in the LBIC scan. An overall linear dependence is found for the three dyes. Similar results are obtained if the scan is performed along different lines or directions or using a different excitation wavelength.

The results in Fig. 9 can be interpreted using the following expression [31]:

$$\mathrm{IPCE} = \mathrm{ECCE} \times \phi_{\mathrm{inj}} \times \mathrm{LHE} = \mathrm{ECCE} \times \phi_{\mathrm{inj}} \times (1 - T - R) \quad (1)$$

where ECCE is the external current collection efficiency, ϕ_{inj} is the injection quantum yield, LHE is the light harvesting efficiency, T the transmittance and R the reflectance. When the other factors are constant, a plot of the IPCE versus the transmittance should give a straight line with a negative slope. This is what is actually found in the LBIC-transmittance data obtained in this study. Furthermore, the slope is observed to be roughly the same for the three dyes, indicating that the injection quantum yield (provided the ECCE is constant) is very similar for the organic dyes and the N719 dye. Note that the reflectance term will introduce a constant shift of the IPCE-transmittance data if we assume that there are no significant differences in the reflectance properties of the film from one point to another. These results confirm that the lower light absorption of the organic dyes due to the narrower absorption spectra is the reason for the somewhat lower efficiencies than obtained for the N719 dye. In light of these results, improvements in the efficiency of cells with organic dyes should be achieved by tailoring the dye chemistry to increase light absorption in the red.

3.5. Stability properties

In order to check the stability of the sealed cells with the xanthene dyes we have measured the photocurrent under continuous illumination at an intensity of 200 mW/cm^2, corresponding to twice the standard solar light intensity. At higher intensity, the turn-over rate of the dye is higher and possible degradation mechanisms could be accelerated. The results are shown in Fig. 10. The stability test revealed that the three dyes studied (N719, Mercurochrome and Eosin Y in its acid form) produce short-circuit photocurrents that are virtually constant. This has been verified for at least 5–8 h and no visible decay is observed over this time span. Stability test were also performed for loaded cells at the

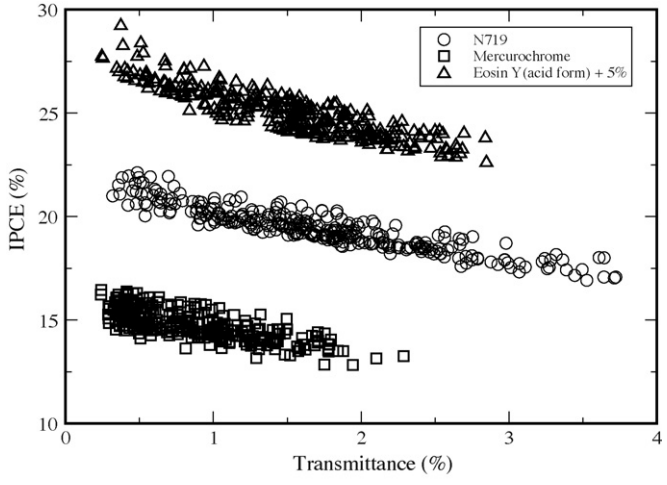

Fig. 9. Quantum efficiency versus transmittance along a single line in a LBIC-transmittance scan with the 532 nm laser. Eosin data are displaced upwards by 5% for clearer presentation.

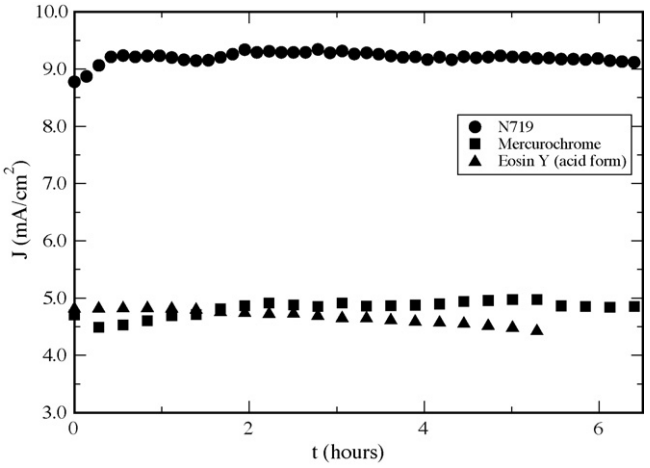

Fig. 10. Photocurrent under short-circuit conditions for sealed cells and different dyes. The illumination intensity was set to 200 mW/cm^2.

maximum voltage point for 2–3 h (not shown). For 200 mW/cm^2 illumination intensity the photocurrent was observed to remain approximately constant in this time interval for Eosin Y and Mercurochrome. It should be noted that the continuous illumination test implies that the cell is heated to approximately 50 °C. In spite of this, the cell remains stable and provides a constant current under continuous illumination. These results indicate that good stability can be obtained with organic dyes, which is essential for the future development of novel DSSC devices.

4. Conclusions

In this work we have compared the performance of dye-sensitised solar cells made with commercial ZnO sensitised with xanthene dyes to the results of cells prepared with the dye of reference, N719. Dyes such as Mercurochrome and eosin can be used to fabricate devices that produce DSSCs with a photovoltaic performance very competitive compared to the N719 dye. The fill factor of N719 cells were shown to deteriorate with sensitisation time. On the contrary, the organic dyes appear more robust in this aspect, such that the efficiency of the N719 cells is easily matched by that of the cells with organic dyes. LBIC and local transmittance measurements show that the main factor that limits the efficiencies of the organic dyes as compared with the N719 reference is their relatively narrow absorption spectrum. Sealed cells with the xanthene dyes show excellent stability properties, even under high illumination intensity conditions. These results are promising and show that, at least for ZnO, commercial organic dyes of the type studied here can be considered as an interesting alternative.

Acknowledgements

We thank the *Ministerio de Educación y Ciencia* of Spain for funding under grants ENE2004 01657 and ENE2007-68040 and project HOPE CSD2007-00007 (Consolider-Ingenio 2010), and Junta de Andalucía under project P06-FQM-01869. G. Oskam thanks the *Consejo Nacional de Ciencia y Tecnología* (CONACYT) of Mexico for funding under project number 43828-Y. We also thank Degussa Spain S.A and DuPont Spain for providing chemicals and materials for research.

References

[1] B. O'Regan, M. Grätzel, A. Low-Cost, High-efficiency solar-cell based on dye-sensitised colloidal TiO_2 films, Nature 353 (1991) 737–740.
[2] M. Grätzel, Photoelectrochemical cells, Nature 414 (2001) 338–344.
[3] Y. Chiba, A. Islam, Y. Watanabe, R. Komiya, N. Koide, L.Y. Han, Dye-sensitised solar cells with conversion efficiency of 11.1%, Japanese Journal of Applied Physics Part 2-Letters & Express Letters 45 (2006) L638–L640.
[4] S.Y. Dai, K.J. Wang, J. Weng, Y.F. Sui, Y. Huang, S.F. Xiao, S.H. Chen, L.H. Hu, F.T. Kong, X. Pan, C.W. Shi, L. Guo, Design of DSC panel with efficiency more than 6%, Solar Energy Materials and Solar Cells 85 (2005) 447–455.
[5] M. Quintana, T. Edvinsson, A. Hagfeldt, G. Boschloo, Comparison of dye-sensitised ZnO and TiO_2 solar cells: studies of charge transport and carrier lifetime, Journal of Physical Chemistry C 111 (2007) 1035–1041.
[6] X. Sheng, Y. Zhao, J. Zhai, L. Jiang, D. Zhu, Electro-hydrodynamic fabrication of ZnO-based dye sensitised solar cells, Applied Physics a-Materials Science & Processing 87 (2007) 715–719.
[7] K. Kakiuchi, E. Hosono, S. Fujihara, Enhanced photoelectrochemical performance of ZnO electrodes sensitised with N-719, Journal of Photochemistry and Photobiology A-Chemistry 179 (2006) 81–86.
[8] K. Keis, C. Bauer, G. Boschloo, A. Hagfeldt, K. Westermark, H. Rensmo, H. Siegbahn, Nanostructured ZnO electrodes for dye-sensitised solar cell applications, Journal of Photochemistry and Photobiology A-Chemistry 148 (2002) 57–64.
[9] L.Y. Zeng, S.Y. Dai, W.W. Xu, K.J. Wang, Dye-sensitised solar cells based on ZnO films, Plasma Science & Technology 8 (2006) 172–175.
[10] K. Keis, E. Magnusson, H. Lindstrom, S.E. Lindquist, A. Hagfeldt, A 5% efficient photo electrochemical solar cell based on nanostructured ZnO electrodes, Solar Energy Materials and Solar Cells 73 (2002) 51–58.
[11] T. Yoshida, K. Terada, D. Schlettwein, T. Oekermann, T. Sugiura, H. Minoura, Electrochemical self-assembly of nanoporous ZnO/Eosin Y thin films and their sensitised photoelectrochemical performance, Advanced Materials 12 (2000) 1214–1217.
[12] W.J. Lee, H. Okada, A. Wakahara, A. Yoshida, Structural and photoelectrochernical characteristics of nanocrystalline ZnO electrode with Eosin-Y, Ceramics International 32 (2006) 495–498.
[13] P. Suri, R.M. Mehra, Effect of electrolytes on the photovoltaic performance of a hybrid dye sensitised ZnO solar cell, Solar Energy Materials and Solar Cells 91 (2007) 518–524.
[14] P. Suri, M. Panwar, R.M. Mehra, Photovoltaic performance of dye-sensitised ZnO solar cell based on Eosin-Y photosensitizer, Materials Science-Poland 25 (2007) 137–144.
[15] J.J. Wu, G.R. Chen, H.H. Yang, C.H. Ku, J.Y. Lai, Effects of dye adsorption on the electron transport properties in ZnO-nanowire dye-sensitised solar cells, Applied Physics Letters (2007) 90, 213109.
[16] K. Hara, T. Horiguchi, T. Kinoshita, K. Sayama, H. Sugihara, H. Arakawa, Highly efficient photon-to-electron conversion with Mercurochrome-sensitised nanoporous oxide semiconductor solar cells, Solar Energy Materials and Solar Cells 64 (2000) 115–134.
[17] M. Matsumura, S. Matsudaira, H. Tsubomura, M. Takata, H. Yanagida, Dye sensitization and surface-structures of semiconductor electrodes, Industrial & Engineering Chemistry Product Research and Development 19 (1980) 415–421.
[18] K. Keis, J. Lindgren, S.E. Lindquist, A. Hagfeldt, Studies of the adsorption process of Ru complexes in nanoporous ZnO electrodes, Langmuir 16 (2000) 4688–4694.
[19] S. Nakade, T. Kanzaki, W. Kubo, T. Kitamura, Y. Wada, S. Yanagida, Role of electrolytes on charge recombination in dye-sensitised TiO_2 solar cell (1): the case of solar cells using the I−/I3(−) redox couple, Journal of Physical Chemistry B 109 (2005) 3480–3487.
[20] E. Guillén, J.A. Anta, A. Vega-Poot, G. Rodriguez-Gattorno, G. Oskam, R. Alcantara, C. Fernandez-Lorenzo, J. Martin-Calleja, Colloidal Zinc oxide for Photovoltaic Applications, 2nd Iberic Meeting of Colloids and Interfaces (RICI2), 2007, p. 59, ISBN: 978-989-8124-01-2.
[21] C. Fernandez-Lorenzo, J.A. Poce-Fatou, R. Alcantara, J. Navas, J. Martin, High resolution laser beam induced current focusing for photoactive surface characterization, Applied Surface Science 253 (2006) 2179–2188.
[22] M.H.J. Rinio, M. Werner, LBIC investigations of the lifetime degradation by extended defects in multicrystalline solar silicon, Solid State Phenomena 63/64 (1996) 115–122.
[23] C.A. Musca, D.A. Redfern, J.M. Dell, L. Faraone, Laser beam induced current as a tool for HgCdTe photodiode characterisation, Microelectronics Journal 31 (2000) 537–544.
[24] F.J. Kao, J.C. Chen, S.C. Shih, A. Wei, S.L. Huang, T.S. Horng, P. Torok, Optical beam induced current microscopy at DC and radio frequency, Optics Communications 211 (2002) 39–45.
[25] P. Salvador, A.M. Chaparro, A. Mir, Digital imaging of the effect of photoetching on the photoresponse of n-type tungsten diselenide and molybdenum diselenide single crystal electrodes, Journal of Physical Chemistry 100 (1996) 760–768.
[26] C.J.L. Moore, C.J. Miner, A spatially resolved spectrally resolved photoluminescence mapping system, Journal of Crystal Growth 103 (1990) 21–27.
[27] A.C. Ribes, S. Damaskinos, H.F. Tiedge, A.E. Dixon, D.E. Brodie, Reflected-light, photoluminescence and OBIC imaging of solar cells using a confocal scanning laser MACROscope/microscope, Solar Energy Materials and Solar Cells 44 (1996) 439–450.
[28] J.A. Poce-Fatou, J. Martin, R. Alcantara, C. Fernandez-Lorenzo, A precision method for laser focusing on laser beam induced current experiments, Review of Scientific Instruments 73 (2002) 3895–3900.
[29] J. Martin, C. Fernandez-Lorenzo, J.A. Poce-Fatou, R. Alcantara, A versatile computer-controlled high-resolution LBIC system, Progress in Photovoltaics 12 (2004) 283–295.
[30] T.P. Chou, Q.F. Zhang, G.Z. Cao, Effects of dye loading conditions on the energy conversion efficiency of ZnO and TiO_2 dye-sensitised solar cells, Journal of Physical Chemistry C 111 (2007) 18804–18811.
[31] J.A. Anta, F. Casanueva, G. Oskam, A numerical model for charge transport and recombination in dye-sensitised solar cells, Journal of Physical Chemistry B 110 (2006) 5372–5378.